GEOPHYSICS, VOL. 81, NO. 5 (SEPTEMBER-OCTOBER 2016); P. T189–T196, 7 FIGS., 1 TABLE.
10.1190/GEO2015-0398.1

Equivalent accuracy at a fraction of the cost: Overcoming temporal dispersion

Yunyue Elita Li[1], Mandy Wong[2], and Robert Clapp[3]

ABSTRACT

Numerical dispersion in finite-difference (FD) modeling produces coherent artifacts, severely constraining the resolution of advanced imaging and inversion techniques. Conventionally, numerical dispersion is reduced by increasing the order of accuracy of the FD operators, and we resign ourselves to paying the high computational cost that is incurred. Assuming no spatial dispersion, we have found that FD time dispersion is independent of the medium velocity and the spatial grid for propagation, and only depends on the time-stepping scheme and the propagation time. Based on this observation, we have devised postpropagation filters to collapse the time-dispersion effect of FD modeling. Our dispersion correction filters are designed by comparing the input waveform with dispersive waveforms obtained by 1D forward modeling. These filters are then applied on multidimensional shot records to eliminate the time dispersion by two schemes: (1) stationary filtering plus interpolation and (2) nonstationary filtering. We have found with 1D and 2D examples that the time dispersion is effectively removed by our postpropagation filtering at a negligible cost compared with a higher order modeling scheme.

INTRODUCTION

Finite-difference (FD) modeling for wave propagation has been widely used for advanced inversion techniques, such as waveform impedance inversion (e.g., Kelly et al., 2010; Plessix and Li, 2013) and full-waveform inversion (e.g., Tarantola, 1987; Virieux and Operto, 2009). In these methods, wavefields modeled by FD are compared with the recorded data. The differences between the modeled and recorded data at large offsets and at late arrival times provide low-wavenumber information of the subsurface, which is crucial to the success of these nonlinear optimization problems. To obtain accurate waveforms, fine FD grids, high-order FD approximations, and small time steps are used to suppress the numerical dispersion. However, these remedies significantly increase the computational cost and memory usage.

Methods to suppress numerical dispersion using lower order FD have been widely studied. Most studies focus on the spatial dispersion, while keeping the time step sufficiently small to mitigate the temporal dispersion. Kosloff and Baysal (1982) use the spatial Fourier transform to eliminate all errors from FD approximation with respect to the spatial derivatives. Fei and Larner (1995) propose to use the flux-corrected transport (FCT) algorithm to reduce the numerical dispersion in FD wavefield continuation. However, the diffusion and antidiffusion processes required by FCT have to be applied at each time step, which increases the computational cost by 80%. Other authors (Holberg, 1987; Fornberg, 1998; Etgen, 2007) have set up optimization objectives to generate different sets of FD coefficients that minimize the misfit between the numerical phase velocity and the theoretical phase velocity for a practical range of frequencies and velocities. Nonetheless, with computational cost controlled by the number of FD coefficients that are optimized, achieving accuracy and efficiency simultaneously is still quite challenging. Moreover, all these methods require a small enough time-stepping size to limit the numerical time dispersion. The accuracy of these methods decreases as the time-stepping size increases.

Recently, Stork (2013) points out that temporal dispersion is independent with velocity and can be removed after propagation. Dai et al. (2014) provide an analytical solution to the temporal dispersion and designed filters accordingly to remove the dispersion artifacts. Due to the nonstationarity, both studies implement time-varying filtering by interpolating multiple filtered traces for each time sample. In this paper, we design these time-variant filters using

Manuscript received by the Editor 23 July 2015; revised manuscript received 14 March 2016; published online 7 July 2016.
[1]Formerly Stanford University, Stanford, California, USA; presently Massachusetts Institute of Technology, Cambridge, Massachusetts, USA. E-mail: yunyueli@mit.edu.
[2]Formerly Stanford University, Stanford, California, USA; presently Shell, Houston, Texas, USA. E-mail: mandyman@sep.stanford.edu.
[3]Stanford University, Stanford, California, USA. E-mail: bob@sep.stanford.edu.

1D modeling results at discrete propagation times. We test two different filtering schemes: (1) stationary filtering plus interpolation (SFPI) (similar to Stork [2013] and Dai et al. [2014]) and (2) nonstationary filtering (NSF). The results show that both postpropagation filtering schemes can eliminate the temporal dispersion on shot records with very low-additional cost. We recommend the NSF scheme for large scale applications due to its higher accuracy and lower memory requirements.

THEORY

Assuming constant density and a source-free medium, the acoustic wave equation may be written as

$$c^2\left(\frac{\partial^2}{\partial x^2}+\frac{\partial^2}{\partial y^2}+\frac{\partial^2}{\partial z^2}\right)P=\frac{\partial^2}{\partial t^2}P, \tag{1}$$

where P is the pressure field and $c(x,y)$ is the velocity.

In FD modeling, both sides of equation 1 are approximated by numerical discretization: the left side in space and the right side in time. Using notation similar to Kosloff and Baysal (1982), the FD equation we are solving is

$$c^2\nabla^2 P^n(i,j,l)=\frac{1}{\Delta t^2}[P^{n+1}(i,j,l)-2P^n(i,j,k)+P^{n-1}(i,j,l)], \tag{2}$$

where $P^n(i,j,l)$ represents the value of the pressure field at time $t=n\Delta t$ and at spatial locations $x=x_0+(i-1)\Delta x$, $y=y_0+(j-1)\Delta y$, and $z=z_0+(l-1)\Delta z$. Symbol ∇^2 represents the Laplacian operator in space, Δt, Δx, Δy, and Δz are the sampling in time and space, respectively. The term $c^2\nabla^2 P^n(i,j,l)$ represents the numerical approximation of the left side.

Equation 2 represents an explicit, second order in time, leap-frog scheme that is widely used in FD modeling implementations. The left and the right sides of equation 2 contain approximation errors with respect to equation 1. We call the error on the left side spatial dispersion and the error on the right side temporal dispersion. Throughout this paper, we focus on reducing the temporal dispersion by fully eliminating the spatial dispersion using a Fourier space implementation for the space derivatives (Kosloff and Baysal, 1982).

Assuming a constant medium, we transform equation 2 to the wavenumber-time domain

$$-c^2k^2\hat{P}^n=\frac{1}{\Delta t^2}[\hat{P}^{n+1}-2\hat{P}^n+\hat{P}^{n-1}], \tag{3}$$

where $\hat{P}$ are the wavefields in the wavenumber domain and $k^2=k_x^2+k_y^2+k_z^2$. We substitute the wavefields with their analytical solutions

$$\hat{P}^{n+1}=\hat{P}^n e^{-i\omega\Delta t}, \tag{4}$$

and obtain the following dispersion relation:

$$c^2=\frac{2-e^{i\omega\Delta t}-e^{-i\omega\Delta t}}{\Delta t^2k^2}=\frac{2(1-\cos(\omega\Delta t))}{\Delta t^2k^2}. \tag{5}$$

Comparing the dispersion relation 5 with the definition of phase velocity

$$c_\phi^2=\frac{\omega^2}{k^2}, \tag{6}$$

we obtain the phase error function of a second-order FD scheme as follows:

$$\phi^{2\text{nd}}=(c_\phi-c)kt=\left(1-\frac{\sqrt{2-2\cos(\omega\Delta t)}}{\omega\Delta t}\right)\omega t. \tag{7}$$

The temporal dispersion increases with stepping size, frequency, and propagation time. Figure 1a shows the waveform modeled in 1D with a second-order time-stepping scheme. The step size in time is 2 ms. Severe time dispersions can be observed as the propagation time increases. The solid lines in Figure 2 plot the phase error by a second-order FD scheme. The progressive positive error at higher frequency agrees with the leading high-frequency dispersion produced by the numerical simulations in Figure 1a.

Conventionally, temporal dispersion can be reduced by increasing the order of the FD for a fixed step size in time. The phase error function for a fourth-order FD approximation (leap-frog scheme) can be shown as follows:

$$\phi^{4\text{th}}=(c_\phi-c)kt=\left(1-\frac{\sqrt{\frac{5}{2}-\frac{8}{3}\cos(\omega\Delta t)+\frac{1}{6}\cos(2\omega\Delta t)}}{\omega\Delta t}\right)\omega t. \tag{8}$$

Figure 1b shows the waveform modeled with a fourth-order time-stepping scheme using the same time increment as in Figure 1a. Severe temporal dispersion artifacts have been almost fully removed. In our straightforward implementation, these results are achieved at twice the computation cost, although the cost of the fourth-order FD method can be partially offset by a larger time step size than the second-order FD (Dablain,

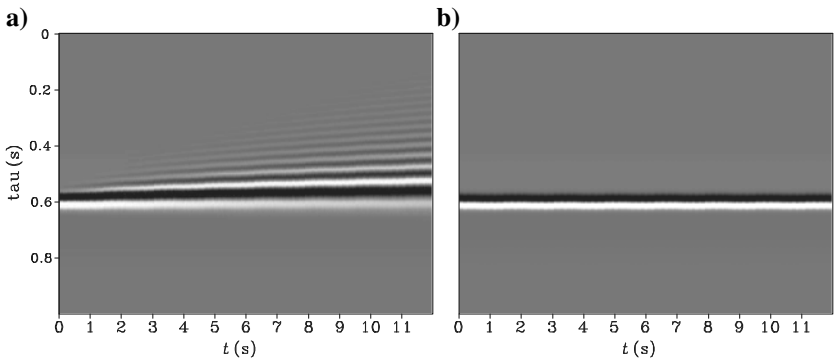

Figure 1. Waveform from 1D modeling using the Fourier method with (a) second-order time stepping and (b) fourth-order stepping. In both cases, we use the same parameters for propagation: $\Delta t=2$ ms, $\Delta x=10$ m, and $v=2000$ m/s. Severe time dispersions are diminished at twice the computation cost and twice the memory.

1986; De Basabe and Sen, 2010). We keep the temporal step size Δt constant to facilitate the comparisons.

The phase error curves for a fourth-order FD scheme (the dotted-dashed line in Figure 2) confirm that the dispersion error is dramatically reduced by an order of magnitude at all frequencies. Despite the slight phase error at high frequencies from a fourth-order FD scheme, the amplitude at these frequencies is so small that the dispersion artifacts are not visible.

Equation 7 suggests that the phase error depends on frequency, propagation time, and the time-stepping size. It is independent of the medium velocity and the spatial grid for propagation when velocity is constant and the spatial discretization is accurate (Stork, 2013; Dai et al., 2014). Therefore, it is feasible to design filters that correct for the phase error after propagation. We use the fourth-order FD modeling results, which are almost dispersion free, as the benchmark for the filtering results.

Instead of estimating the filters based on the analytical phase error function 7, as suggested by Dai et al. (2014), we estimate the filters numerically from 1D modeling. We compare the waveform $s_i(t)$ at propagation time t_i with the source waveform $s_0(t)$ in the Fourier space:

$$F(\omega, t_i) = \frac{S_i(\omega)}{S_0(\omega) + \epsilon}, \tag{9}$$

where $S_i(\omega)$ and $S_0(\omega)$ are the Fourier representation of $s_i(t)$ and $s_0(t)$, respectively. A small number $\epsilon = 10^{-7}$ is added to stabilize the division. Filter $F(\omega, t_i)$ or its time representation $f(\tau, t_i) = \mathcal{F}^{-1}F(\omega, t_i)$ can be applied in Fourier or time domain to correct for the temporal dispersion. Note that the filter coefficients $f(\tau, t_i)$ at different filter lags τ are determined by the propagation time t_i.

Figure 3 shows the filters obtained numerically from equation 9 at discrete propagation times. The 10 filters are estimated every second by comparing the modeled waveforms in Figure 1a with the initial waveform. The increasing negative phase shift (time delay) is needed to compensate for the increasing positive phase error as the propagation time increases. Figure 2 compares the phase error estimated from equation 9 with the analytical phase error function from equation 7. The numerical estimation of the phase error agrees very well with the analytical solution.

To apply these sparse filters on densely sampled (in time) data record, we can choose from the following two schemes: SFPI or NSF. Both methods are applied trace-by-trace. Therefore, it can be applied very efficiently in parallel on 2D or 3D data.

SFPI

Given a modeled record $d(t, x)$, we can first convolve each of the filters to the whole record

$$d_i(t, x) = d(t, x) * f(\tau, t_i), \tag{10}$$

by a trace-by-trace operation to obtain multiple copies of the data record. On each filtered record $d_i(t, x)$, only the waveforms around $t = t_i$ are correctly filtered. The other parts of the record are either over or under compensated. We then interpolate among the filtered records to obtain the dispersion-free record $\hat{d}(t, x)$

$$\hat{d}(t, x) = \sum_i^N h_i d_i(t, x), \tag{11}$$

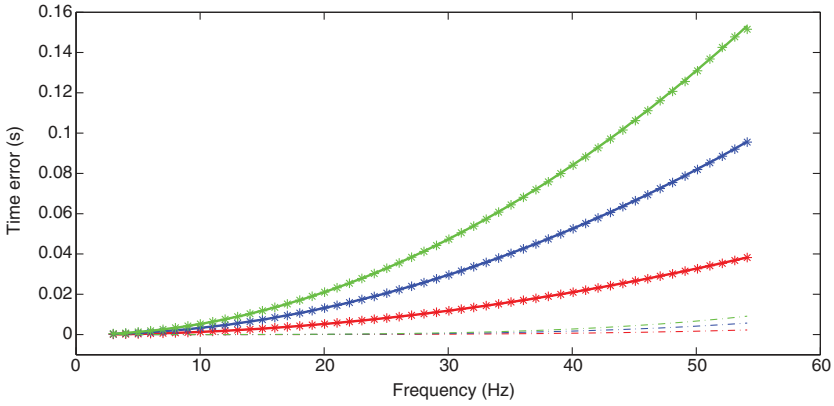

Figure 2. Solid lines plot the frequency dependent phase error by a second-order FD modeling scheme. Dotted dash lines plot the error by a fourth-order FD modeling scheme. The asterisks denote the estimated phase error from the numerical filters. The red, blue, and green color denotes the phase error at $t = 2$, 5, and 8 s, respectively.

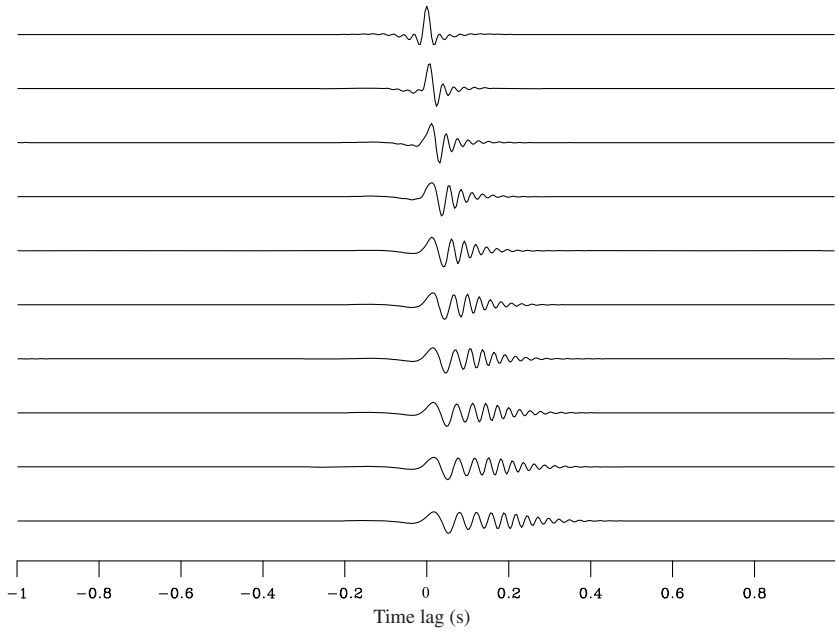

Figure 3. The 10 filters estimated every second by comparing the waveforms modeled by second-order time-stepping scheme in Figure 1a with the initial waveform. The increasing negative phase shift (time delay) is needed to compensate for the increasing positive phase error as the propagation time increases.

where N is the total number of filters and $h(i)$ are the linear interpolation weights for the filtered records

$$h(i) = \begin{cases} \frac{t-t_i}{t_{i+1}-t_i}, & \text{if } t_i < t < t_i + 1 \\ 0, & \text{otherwise} \end{cases}. \tag{12}$$

NSF

In the NSF scheme, we choose a moving window W_i, which has the same length as the filter, to select the data patch to convolve with the filter defined at the center of the moving window. We overlap the moving windows to ensure smooth transitions across the data patch. Mathematically, the filtering process can be formulated as follows:

$$\hat{d}(t,x) = \frac{1}{N}\sum_{i}^{N}(W_i d(t,x)) * f(\tau, t_i^w), \tag{13}$$

where W_i is the ith window of length l selecting the data trace

$$W_i(t) = \begin{cases} 1, & \text{if } |t_i^w - t| \le l/2 \\ 0, & \text{otherwise} \end{cases}. \tag{14}$$

In the numerical examples, we use $l = 1$ s, $N = 8$. Therefore, the filters are needed at every 0.125 s.

According to equation 7, the dispersion varies linearly with propagation time. Hence, we build the filters at any propagation time by interpolating the estimated filters as follows:

$$f(\tau, t_i^w) = \sum_{i}^{N} h(i) f(\tau, t_i). \tag{15}$$

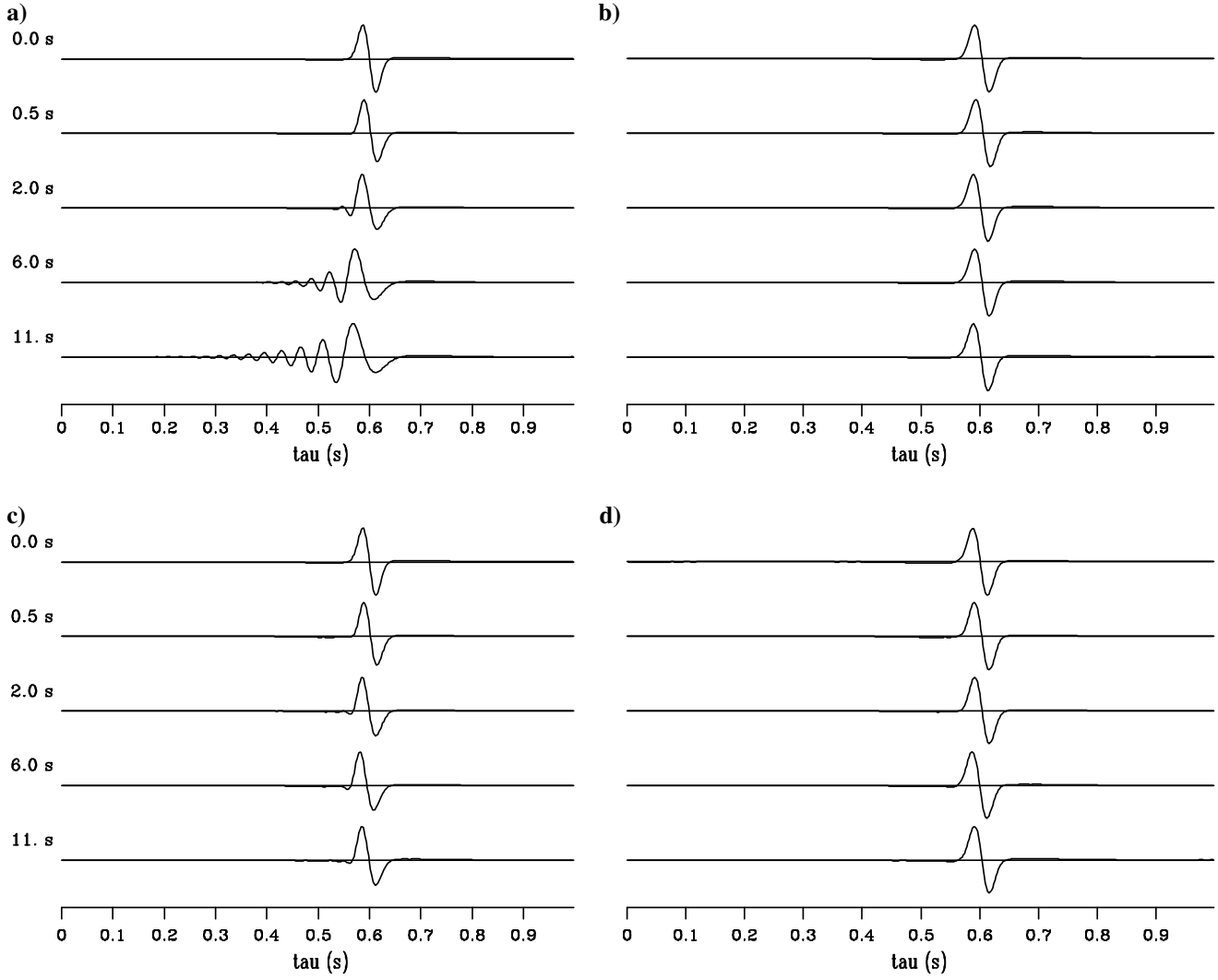

Figure 4. The 1D modeling and filtering results with 6 m spacing and 1000 m/s velocity. Waveforms are shown after being propagated for 0, 0.5, 2, 6, and 11 s. (a) Second-order time-stepping results. Dispersion gets greater with propagation time. (b) Fourth-order time-stepping results. Dispersion is almost fully eliminated at twice the cost of second-order time stepping. (c) Second-order time-stepping results after dispersion correction by SFPI. Results show residual dispersion effects due to the limited number of filters used for processing. (d) Second-order time-stepping results after dispersion correction by NSF.

More advanced NSF schemes (Margrave, 1997; Fomel, 2009) can be adapted in practice; however, in the examples we present here, this simple patching method yields satisfactory results.

NUMERICAL EXAMPLES

We test the proposed postpropagation filtering schemes on 1D and 2D examples. All spatial derivatives in the numerical modeling are performed in the Fourier space to eliminate the spatial dispersion.

Table 1: Runtime for different numerical methods.

Method	Second order	Fourth order	Second order and SFPI	Second order and NSF
Runtime (s)	61.99	115.82 (80.32)	62.36	62.47

Figure 4a and 4b shows the second- and fourth-order modeling results with $\Delta t = 2$ ms, $\Delta x = 6$ m/s, and $v = 1000$ m/s. Dispersion is greatly reduced by the fourth-order modeling scheme at twice the computational cost and memory usage. We use the filters in Figure 3a to process the second-order modeling results. Notice that the spatial grid and propagation velocity are different when estimating the filters. Figure 4c and 4d shows that the numerical dispersion has been removed after filtering and the dispersion correction filters are effective as long as the time step Δt remains the same.

Figure 5 shows the modeling and filtering results on a modified 2D Marmousi model with a 500 m water column. Magnified views to large offsets and late arrival times are shown in Figure 6. We use 25 m spacing for both spatial directions, and 2 ms time stepping, which is 88% of the Courant-Fridrichs-Lewy (CFL) condition (Courant et al., 1928). Execution time with 2 ms time step for each method is reported in Table 1. For the fourth-order method, we also record the runtime with 3 ms time step between the brackets. Our straightforward implementation shows that the postpropagation filtering adds negligible cost to the original second-order time-stepping scheme.

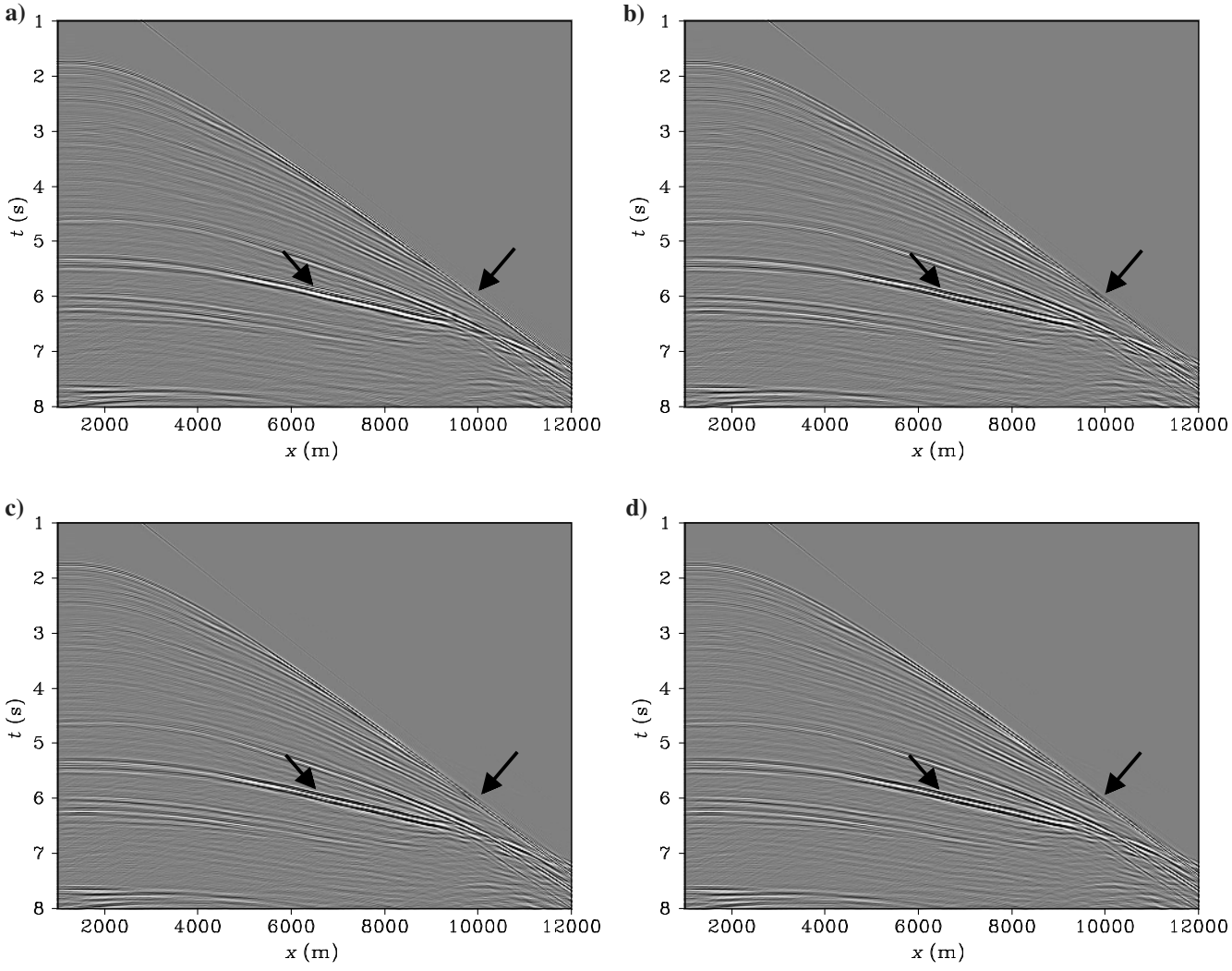

Figure 5. A shot record by 2D modeling. (a) Shot record with second-order FD propagation. (b) Shot record with fourth-order FD propagation. Dispersion artifacts are almost fully eliminated at twice the cost of a second-order scheme. (c) Shot record (a) after dispersion correction by SFPI. (d) Shot record (a) after dispersion correction by NSF. The dispersion effects are corrected by postpropagation filtering.

The red arrows in Figures 5a and 6a point to parallel events leading the main events that are clearly temporal dispersion artifacts. The proposed postpropagation filtering schemes remove these artifacts and produce close approximations to the fourth-order modeling results.

Figure 7 shows the late waveforms at a single receiver $x = 10{,}000$ m modeled using different schemes. The waveform modeled by standard second-order FD propagation is severely dispersed that waveform-based inversion scheme would lead to erroneous results (Figure 7a). Postpropagation filtering restores the phase of the waveform at negligible additional cost. Comparisons with fourth-order modeling between SFPI (Figure 7b) and NSF (Figure 7c) schemes indicate that amplitude and phase filtered by NSF better approximate the fourth-order modeling results.

DISCUSSION

We presented two filtering schemes: SFPI and NSF in this paper. Both methods only involve 1D filtering in time, the computational cost of which does not depend on the size of the computational grid. The length of the filter has to permit dispersion corrections that at the maximum propagation time, which can be empirically determined by the 1D waveforms when building the filters. The NSF scheme is 30% more expensive than the SFPI scheme; however, both schemes on a single shot record cost less than 0.5% of the computational time for wave simulation. Moreover because the filtering process is independent for each trace, both schemes can be implemented in parallel, which would further reduce the computational cost to virtually negligible.

Although the filtering results of both schemes are similar, the SFPI scheme results in more residual dispersion compared with the NSF scheme, given the same number of filters. The NSF scheme, with the extra interpolation between the filters, has effectively estimated the filters every $1/8$ s, resulting in more accurate filtering results in phase and amplitude. Furthermore, the SFPI scheme interpolates among multiple copies of the data record, which may require large input-output (IO) and memory usage. Therefore, considering the accuracy and memory requirements, we recommend the NSF scheme over the SFPI scheme.

Our method can be readily applied to accurately model the synthetic seismograms with low cost, which is crucial when matching the synthetic data with the long offset, broadband field recordings.

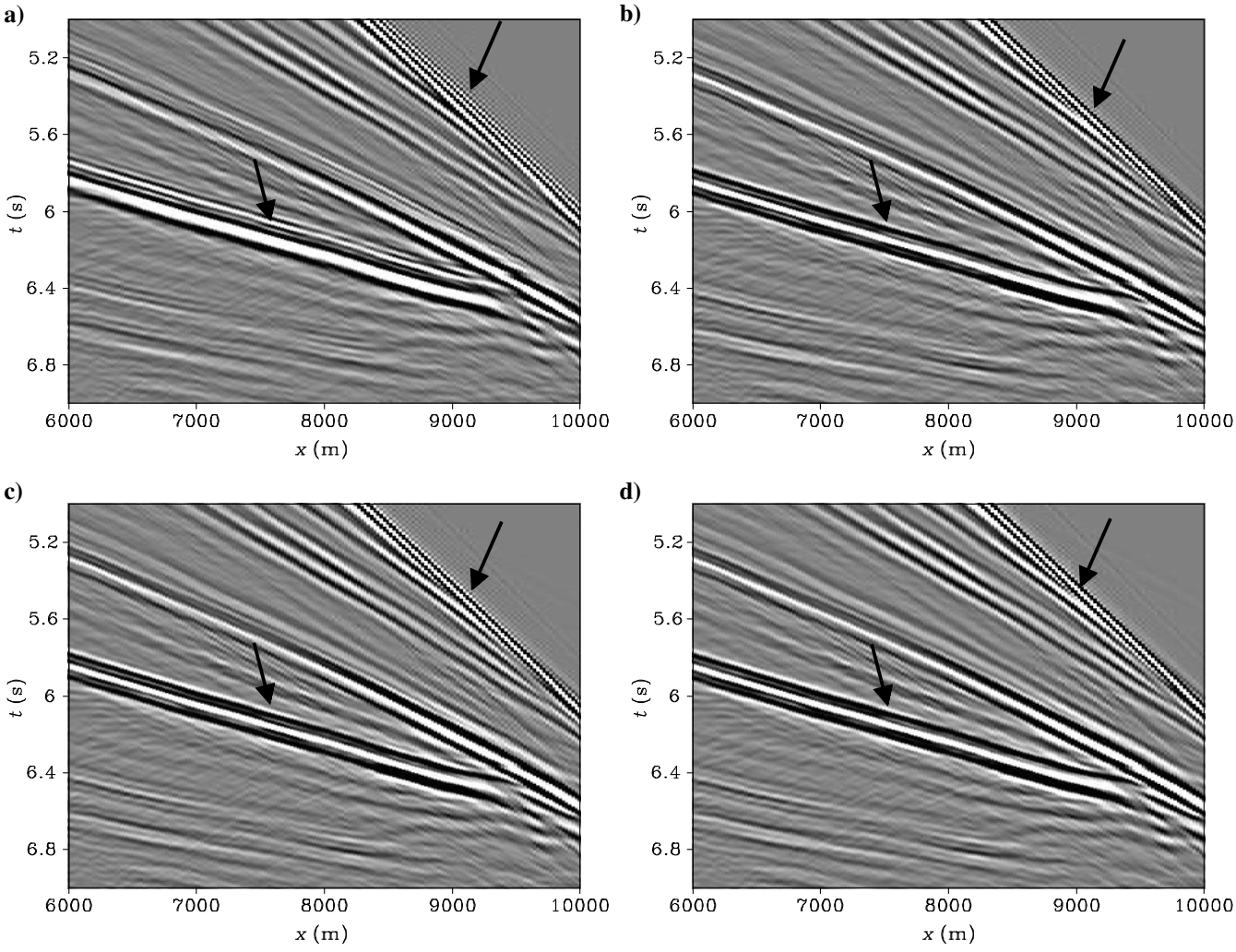

Figure 6. Magnified view of Figure 5 at a late time and large offsets.

Although the filtering schemes become less accurate with imperfect spatial FD approximation, they can be incorporated with high order, optimized, or low rank spatial FD schemes (e.g., Etgen, 2007; Fomel et al., 2013; Dai et al., 2014) to further decrease the computational cost and increase the time-stepping size.

The proposed methods also suggest a preprocessing step for reverse time migration (RTM) to overcome the numerical dispersion caused by the low-order FD in time. Zhang et al. (2013) and Dai et al. (2014) provide numerical examples to demonstrate this idea. Here, we illustrate the effectiveness of this method analytically. Prior to RTM, we filter the data $d(\omega) = e^{-i\omega t_0}$ (space coordinates are ignored for simplicity) using the inverse of the filters $f^{-1}(\omega, t_0) = e^{i\phi^{2\text{nd}}(\omega,t_0)}$. The filtered data are

$$d_f(\omega) = e^{-i\omega t_0} e^{i\phi^{2\text{nd}}(\omega,t_0)}. \tag{16}$$

In RTM, the receiver wavefield is modeled by propagating the recorded data backward in time:

$$R(\omega) = d_f(\omega) e^{i\omega t_r} e^{-i\phi^{2\text{nd}}(\omega,t_r)}, \tag{17}$$

where t_r is the propagation time between the receiver location and the imaging point, and $e^{-i\phi^{2\text{nd}}(\omega,t_r)}$ denotes the numerical dispersion during propagation. Similarly, the source wavefield is

$$S(\omega) = w(\omega) e^{-i\omega t_s} e^{i\phi^{2\text{nd}}(\omega,t_s)} \tag{18}$$

with t_s the propagation time between the source location and the imaging point. The image is obtained based on the crosscorrelation imaging condition (Claerbout, 2008):

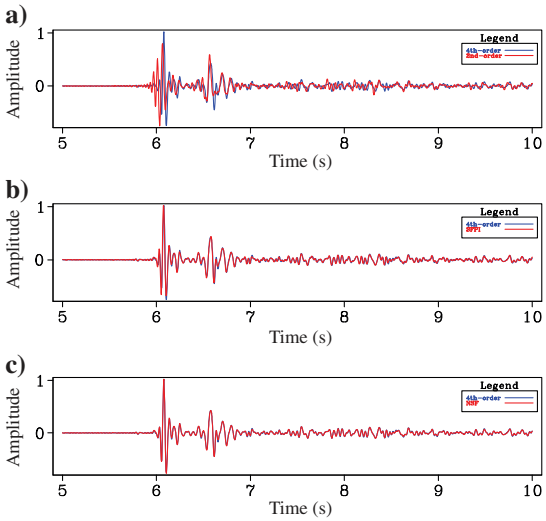

Figure 7. Single-trace comparison at receiver $x = 10{,}000$ m by 2D modeling. (a) Comparison between the second-order (red) and the fourth-order (blue) modeling results. Second-order model result shows leading dispersion artifacts. (b) Comparison between the SFPI filtered result (red) and the fourth-order modeling (blue) result. (c) Comparison between the NSF filtered result (red) and the fourth-order modeling (blue) result. Postpropagation filtering removes the numerical dispersion at negligible additional cost.

$$\begin{aligned} I &= \sum_{\omega} S(\omega)\overline{R(\omega)} \\ &= \sum_{\omega} w(\omega) e^{-i\omega(t_r+t_s-t_0)} e^{-i(\phi^{2\text{nd}}(\omega,t_0)-\phi^{2\text{nd}}(\omega,t_r)-\phi^{2\text{nd}}(\omega,t_s))}. \end{aligned} \tag{19}$$

The stationary phase contribution at the imaging point ensures that $t_0 = t_s + t_r$, which along with the linear relation between propagation time and the phase error (equation 7), leads to cancellation of the numerical dispersion at the imaging point:

$$\phi^{2\text{nd}}(\omega, t_0) = \phi^{2\text{nd}}(\omega, t_r) + \phi^{2\text{nd}}(\omega, t_s). \tag{20}$$

Therefore, applying the inverse of the filters on recording data prior to RTM is effectively delaying the phase of the recording data, such that the numerical dispersion caused by source and receiver propagation cancels at the imaging point.

CONCLUSION

We have developed two postpropagation filtering schemes to remove the temporal dispersion caused by the inaccuracy of the second-order FD approximation to the time derivatives when solving the wave equation. Numerical tests on 1D and 2D modeling examples show that both filtering schemes sufficiently remove the dispersion artifacts at negligible additional cost. As a result, both filtering schemes permit low-order FD in time to achieve high numerical accuracy.

ACKNOWLEDGMENTS

The authors acknowledge the sponsors of the Stanford Exploration Project for their financial support. The authors acknowledge E. Zhebel and two anonymous reviewers for insightful suggestions.

REFERENCES

Claerbout, J. F., 2008, Basic earth imaging: Citeseer.
Courant, R., K. Friedrichs, and H. Lewy, 1928, Über die partiellen Differenzengleichungen der mathematischen Physik: Mathematische Annalen, **100**, 32–74, doi: 10.1007/BF01448839.
Dablain, M. A., 1986, The application of higher-order differencing to the scalar wave equation: Geophysics, **51**, 54–66, doi: 10.1190/1.1442040.
Dai, N., H. Liu, and W. Wu, 2014, Solutions to numerical dispersion error of time FD in RTM: 84th Annual International Conference, SEG, Expanded Abstracts, 2369–2373.
De Basabe, J. D., and M. K. Sen, 2010, Stability of the high-order finite elements for acoustic or elastic wave propagation with high-order time stepping: Geophysical Journal International, **181**, 577–590.
Etgen, J., 2007, A tutorial on optimizing time domain finite-difference schemes: "Beyond Holberg": SEP report 129, 33–43.
Fei, T., and K. Larner, 1995, Elimination of numerical dispersion in finite-difference modeling and migration by flux-corrected transport: Geophysics, **60**, 1830–1842, doi: 10.1190/1.1443915.
Fomel, S., 2009, Adaptive multiple subtraction using regularized nonstationary regression: Geophysics, **74**, no. 1, V25–V33, doi: 10.1190/1.3043447.
Fomel, S., L. Ying, and X. Song, 2013, Seismic wave extrapolation using low-rank symbol approximation: Geophysical Prospecting, **61**, 526–536, doi: 10.1111/gpr.2013.61.issue-3.
Fornberg, B., 1998, Calculation of weights in finite difference formulas: SIAM Review, **40**, 685–691, doi: 10.1137/S0036144596322507.
Holberg, O., 1987, Computational aspects of the choice of operator and sampling interval for numerical differentiation in large-scale simulation of wave phenomena: Geophysical Prospecting, **35**, 629–655, doi: 10.1111/gpr.1987.35.issue-6.

Kelly, S., J. Ramos-Martinez, B. Tsimelzon, and S. Crawley, 2010, Application of an impedance-based full-waveform inversion method for dual-sensor single streamer field recordings: 72nd Annual International Conference and Exhibition, EAGE, Extended Abstracts, A020.

Kosloff, D. D., and E. Baysal, 1982, Forward modeling by a Fourier method: Geophysics, **47**, 1402–1412, doi: 10.1190/1.1441288.

Margrave, G., 1997, Nonstationary filtering: Review and update: CREWES Research Report, 9.

Plessix, R. E., and Y. Li, 2013, Waveform acoustic impedance inversion with spectral shaping: Geophysical Journal International, **195**, no. 1, 301–314.

Stork, C.., 2013, Eliminating nearly all dispersion error from FD modeling and RTM with minimal cost increase: 75th Annual International Conference and Exhibition, EAGE, Extended Abstracts, Tu 11 07.

Tarantola, A., 1987, Inverse problem theory: Methods for data fitting and model parameter estimation: Elsevier Science Publication Company, Inc.

Virieux, J., and S. Operto, 2009, An overview of full waveform inversion in exploration geophysics: Geophysics, **74**, no. 6, WCC1–WCC26, doi: 10.1190/1.3238367.

Zhang, L., G. Shan, and Y. Wang, 2013, System and method for seismic data modeling and migration: U.S. Patent US8614930 B2.